ACS Sustainable Chemistry & Engineering

pubs.acs.org/journal/ascecg

Research Article

Downloaded via XIAMEN UNIV on July 13, 2022 at 06:37:49 (UTC).
See https://pubs.acs.org/sharingguidelines for options on how to legitimately share published articles.

From Mosaic-Type to Heterojunction-Type SEI Films on the Li Anode: Decoupling Chemical and Electrochemical Degradation of the Electrolyte

Jiaxiang Liu, Nanbiao Pei, Haiming Hua, Yi Deng, Haoshen Ma, Peng Zhang,* and Jinbao Zhao*

Cite This: https://doi.org/10.1021/acssuschemeng.2c02668

Read Online

ACCESS | Metrics & More | Article Recommendations | Supporting Information

ABSTRACT: The solid electrolyte interphase (SEI) film is vital to the plating/stripping behavior of lithium metal, while the formation mechanism has not been explained clearly. Here, the formation process of the SEI film is first classified into chemical and electrochemical degradation routes by introducing a LiZn alloy, a chemically inert but electrochemically reactive interphase, as a distinguished research substrate. In a carbonate electrolyte, it is found that the common inorganic matters (such as Li_2O and LiF) mainly originate from the chemical degradation of the electrolyte; meanwhile, the electrochemical degradation mainly generates organic species such as C-OR and COOR. Based on this understanding, the SEI film can be further accurately regulated, and a heterojunction-type SEI film with a well-defined composition and structure is constructed. This offers us a new perspective to understand and regulate the formation of the SEI film for applicable lithium metal batteries.

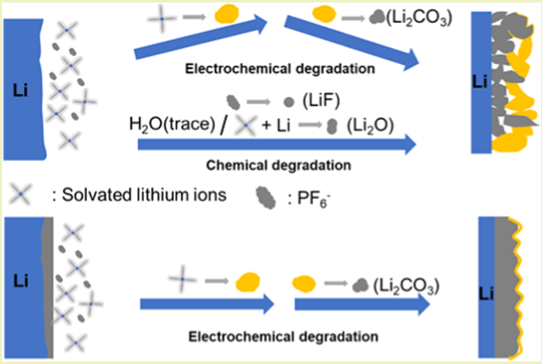

KEYWORDS: *lithium metal anode, LiZn alloy layer, chemical degradation, electrochemical degradation, accurate regulation*

INTRODUCTION

Rechargeable lithium metal batteries (LMBs) have always been considered as an alternative with higher energy density for lithium-ion batteries, as the lithium metal anode has a high theoretical specific capacity (3860 mAh g^{-1}) and the lowest redox potential (−3.04 V vs SHE).[1−3] Unfortunately, the application of lithium metal anodes is limited by the low cycle reversibility and potential safety trouble caused by the uncontrolled growth of lithium dendrites.[4−6] The key issue is the high chemical and electrochemical reactivity between the lithium metal anode and the electrolyte, which can promote the uncontrollable formation of a solid electrolyte interphase (SEI) film.[7−9] The uneven interphase can induce the irregular nucleation of lithium, and the defects of the SEI film would also cause electrochemical hot spots, eliciting lithium dendrites.[10,11] Hence, regulation of the SEI film via the rational design of the electrolyte[12,13] or the preconstruction of an artificial SEI film[14] has been widely explored.

The composition and structure of the SEI film are crucial to the reversible plating/stripping behavior of the lithium metal anode. According to the generally accepted structure and components, the SEI film can be depicted as the mosaic model with a dual-layer structure and various components.[15,16] However, the complexity of the degradation route of the electrolyte hinders the precise regulation of the SEI film. Due to the low redox potential of lithium metal, many components of the organic liquid electrolytes, such as solvent and salt, will undergo irreversible degradation during the plating/stripping of lithium metal.[17] However, the formation of the SEI film during this process is actually the coupling of chemical and electrochemical reactions, while many previous research studies have not carefully distinguished between these two routes.[18] During the common plating/stripping of lithium, the electrolyte will be continuously decomposed electrochemically due to the uninterrupted current and polarization, which can be identified as the electrochemical degradation route of the electrolyte. Furthermore, when a large amount of lithium metal is plated, it will also react with the electrolyte directly due to its high activity, which occurs along with the electrochemical degradation. This direct reaction between the fresh lithium metal and the electrolyte could be identified as the chemical degradation route of the electrolyte.[19−21] These two routes are ineluctably a couple of coupling and competitive procedures during the cycle of lithium metal batteries, which determine the composition and structure of the SEI film. However, the coupling chemical and electrochemical degradation of the

Received: May 4, 2022
Revised: June 24, 2022

© XXXX American Chemical Society

electrolyte is hard to be distinguished due to the fast reactive characteristics of lithium metal.

Herein, a LiZn alloy layer with high chemical resistance and fast charge transfer kinetics was introduced to the surface of the lithium metal foil to distinguish between the chemical and electrochemical degradation of the electrolyte. Based on the handy distinction of these two degradation routes, the SEI film with well-defined components and a well-defined structure can be further constructed. The chemical degradation accompanied with electrochemical degradation will form the traditional mosaic SEI film with diverse inorganic and organic components mixed together (Scheme 1a). However, once the chemical reaction is suppressed by the preconstructed LiZn alloy as the interphase, the SEI film can be further regulated with high organic purity by electrochemical modification (Scheme 1b). Hence, a heterojunction-type SEI film with dual-functional layers, each of which possesses a distinct but synergistic feature, is constructed.

Scheme 1. (a) Formation Process of the SEI Film on the Li Foil after the Electrochemical Treatment. (b) Formation Process of the Heterojunction-type SEI Film by Electrochemical Modification

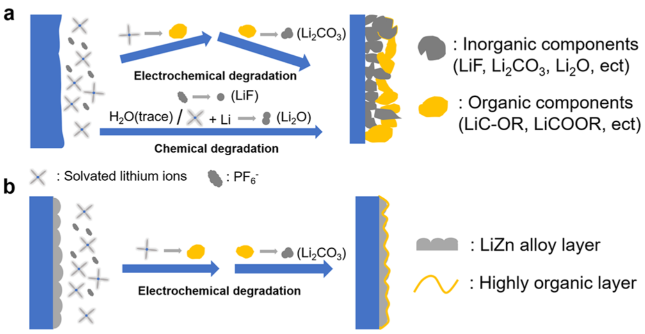

EXPERIMENTAL SECTION

Construction of the LiZn Layer. A total of 3.6 g of zinc trifluoromethanesulfonate (ZnTFS, Aladdin, Shanghai) was dissolved in 100 mL of tetrahydrofuran (THF, Aladdin, Shanghai) to prepare 0.1 M ZnTFS solution. Then, lithium foil was polished until the surface was shining and immersed in 1 M ZnTFS solution for 20 s. After that, it was washed using THF to clean and dried for 24 h under vacuum. All the above-mentioned operations were performed in a glovebox filled with argon, with H_2O and O_2 concentrations below 0.5 ppm.

Construction of the Heterojunction-Type SEI Film. The modified Li foil with the inner LiZn layer was assembled as a half cell with the LiZn foil as the counter electrode and stainless steel as the working electrode. Then, the heterojunction-type SEI film is formed by charging it within 1.1−1.6 V at a scan rate of 0.5 mV for three cycles, wherein the electrolyte is 1 M lithium hexafluorophosphate ($LiPF_6$) dissolved in ethylene carbonate (EC) and dimethyl carbonate (DEC), 1:1 volume ratio with 5 wt % vinylene carbonate (VC) additive as the electrolyte. The treated Li foil was taken out and washed using DEC three times and dried under vacuum for use. The assembly and disassembly of the batteries were carried out in a glovebox filled with argon gas, with H_2O and O_2 concentrations below 0.5 ppm.

Materials and Electrochemical Characterization. XRD patterns were measured using an X-ray diffractometer (Rigaku, Miniflex 600, Cu Kα, $\lambda = 0.154$ nm). The morphology and elemental distribution were obtained by scanning electron microscopy (HITACHI, TM3030) and energy dispersive X-Ray spectroscopy (Oxford, AZTECONE). The analysis of the composition was conducted by X-ray photoelectron spectroscopy (Thermo Fisher, Escalab Xi+), and the samples were etched using Ar, wherein the speed is 0.2 nm/s for a standard sample. The in situ observation images of lithium deposition were obtained using in situ microscopic imaging of batteries (Beijing Scistar Technology Co. Ltd, LIB-MS-II). The electrochemical performance of the modified anode was tested in coin cells. All coin cells (CR2025) were assembled in a glovebox (Ar, $O_2 < 0.5$ ppm, $H_2O < 0.5$ ppm) with Celgard 2500 separators, wherein the electrolyte is 1 M $LiPF_6$ (EC/DEC = 1:1, 5 wt % VC). Next, 75 μL of electrolyte was added to each coin. The electrochemical impedance was measured from 0.1 Hz to 100 kHz

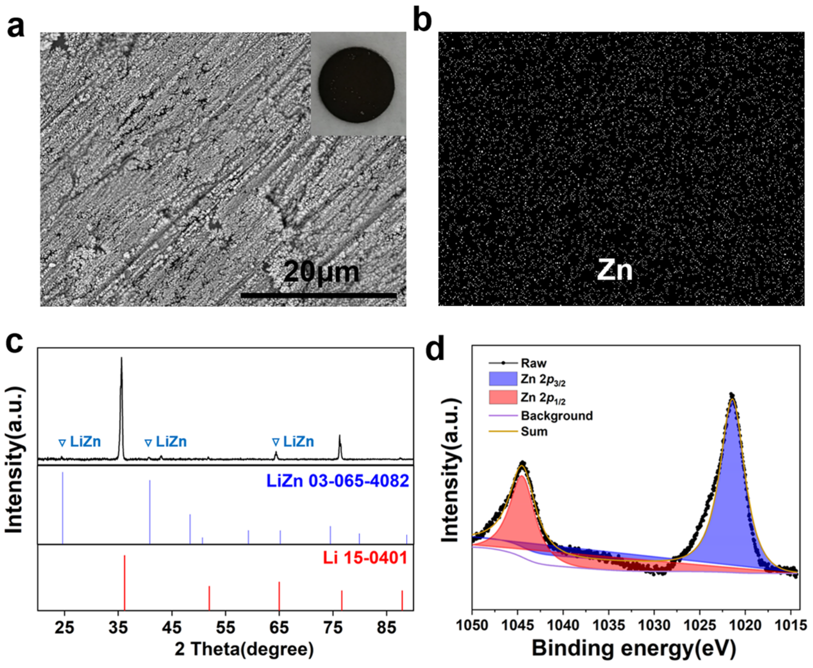

Figure 1. Optical and SEM image (a) and elemental mapping (b) of the LiZn foil. (c) XRD pattern of the surface of the LiZn foil. (d) Curve fit of the Zn 2p XPS spectrum of the surface of LiZn foil.

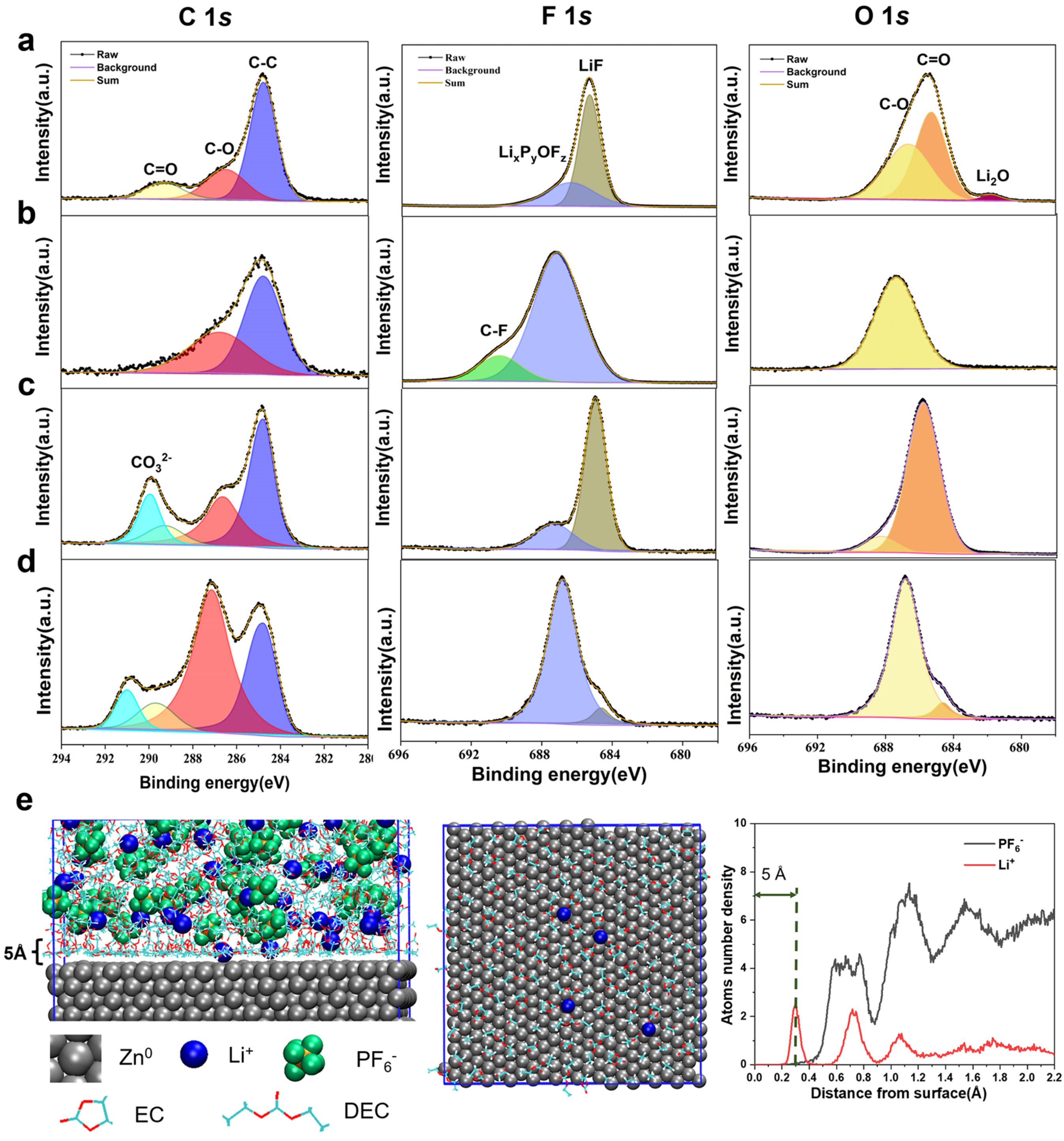

Figure 2. (a) XPS spectrum of the surface of the polished Li foil after exposing to the carbonate-based electrolyte for 72 h. (b) XPS spectrum of the surface of the LiZn foil after exposing to the carbonate-based electrolyte for 72 h. (c) XPS spectrum of the surface of the polished Li foil after CV scanning for three cycles. (d) XPS spectrum of the surface of the polished LiZn foil after CV scanning for three cycles. (e) Ion distribution near the LiZn interphase when cathodic polarization of −200 mV vs PZV is applied.

by electrochemical impedance spectroscopy (Solartron, Modulab 1260). The Nyquist plots with one semicircle can be interpreted using series-wound equivalent analogues of retractor−capacitor (RC) circuits in series, while the semicircle diameter is proportional to the interface impedance of the SEI film. The Tafel curves afre obtained by scanning with a potential range of −0.13 to 0.13 V with a scanning rate of 0.1 mV/s, and the exchange current density is calculated from the Tafel curves.

Computational Details. The restrained electrostatic potential[22] (RESP) atom charges were calculated at the B3LYP-D3[23,24]/def2svp[25] theoretical level using Gaussian09E01[26] and Multiwfn[27,28] software tools.

Molecular dynamics (MD) simulation was performed using Gromacs2018.8[29] software to study the Zn/LB-302 interface at different potentials. The OPLS-AA force field parameters of PF_6^-, DEC, and EC were created with the Acpype program.[30] The Leonard-Jones parameters of metal zinc atoms were set as $\sigma = 2.44$ Å and $\varepsilon = 1.511$ kJ/mol. RESP atom charges were used to describe electrostatic interactions. Atomic charges of all ions were multiplied by a scale factor of 0.78 to correct the polarization effect of ions. A constraint

https://doi.org/10.1021/acssuschemeng.2c02668

potential (force constant = 1 × 10^5 kJ/mol) in the *x*, *y*, and *z* axes for Zn atoms in the electrode was used to maintain the structure of metallic zinc. The electrode potential was controlled by the charge density of the zinc metal surface. The interface capacitance was set to 40 μF/cm^2.

An 8-layer slab containing 3680 Zn atoms was used as the model of the [001] surface of the Zn electrode. The boxes of 302 electrolyte were built by filling 80 Li^+, 80 PF_6^-, 595 EC, and 307 DEC. The boxes were first submitted to energy minimization using the steepest descent method. Equilibrium simulation was carried out with the NPT ensemble at 298.2 K and 1 bar for 20 ns; production simulation was carried out with the NVT ensemble at 298.2 K for 20 ns. The distribution of number density was calculated using Gromacs2018.8. VMD[31] software to visualize the systems.

■ RESULTS AND DISCUSSION

The LiZn alloy layer is introduced to the surface of the Li foil via a simple chemical reaction. Figure 1a,b manifests that the constructed LiZn alloy layer is homogeneous and dense, which can act as a desirable interphase. The corresponding peaks of XRD in Figure 1c show the XRD patterns of the treated LiZn foil. Peaks at 24.7, 40.9, and 65.2° correspond well to the (111), (220), and (331) planes of the LiZn alloy, respectively,[32] confirming the formation of the LiZn alloy layer after such a chemical reaction. The other sharp peaks can be attributed to the metallic lithium. The XPS spectrum of Zn 2p (Figure 1d) also attests the formation of the LiZn alloy layer in which the two peaks at 1021.6 and 1044.5 eV can be assigned to Zn $2p_{3/2}$ and Zn $2p_{1/2}$, respectively.[33] To verify the chemical reaction characteristic of different anode materials, polished pure Li foil and LiZn foil were assembled as symmetrical cells and shelved to observe the calendar aging process. The LiZn foil exerts negligible variation of impedance over time (Figure S1a), while the impedance of the polished lithium foil increases rapidly, from 119.43 to 191.66 Ω for just 24 h (Figure S1b). This demonstrates that the LiZn alloy layer is a highly chemically inert layer, which can suppress the direct chemical degradation of the electrolyte and delay the calendar aging process of the lithium metal anode. Meanwhile, the LiZn alloy layer is not a strictly electrically insulated interphase; the electrochemical degradation of the electrolyte would still happen due to the constant current and polarization. This characteristic provides an excellent model for distinguishing between and exploring the electrochemical degradation and chemical degradation of the electrolyte. Herein, the LiZn alloy layer is applied as a chemically inhibited but electrochemically favored interphase to further explore the detailed formation mechanism of the SEI film.

The degradation of the electrolyte was explored in common carbonate electrolytes with EC and DEC as solvents, $LiPF_6$ as the salt, and VC as an additive. The chemical degradation of the electrolyte was observed by placing the polished Li foil and LiZn foil in the electrolyte for 72 h. XPS analysis is performed on the immersed lithium foil to determine the decomposition species (Figure 2a,b). As shown in the C 1s spectra, the peaks centered at around 284.8, 286, and 289.3 eV can be, respectively, ascribed to C-C, C-OR, and COOR.[34] The commonly observed C-C and C-OR species appear in both the Li foil and LiZn foil. In particular, C 1s spectra show that the COOR species is not found in the LiZn foil (Figure 2b), signifying that the degradation of the electrolyte forming COOR can be significantly inhibited. According to F 1s spectra, the peaks centered at around 684.8 and 687 eV correspond to LiF and $Li_xP_yOF_z$, respectively, which are commonly regarded as the chemical decomposition products of $LiPF_6$.[35,36] It is represented that LiF is absent on the surface of the LiZn foil (Figure 2b) compared to the Li foil (Figure 2a), certifying the desirable chemically inert characteristic of the LiZn alloy layer. O 1s spectra also manifest that C=O (~531.1 eV) and LiO_2 (~528.1 eV) are not observed on the LiZn foil (Figure 2b) compared to the Li foil (Figure 2a).[37] It could clearly be attributed to the fact that the species on the surface of the chemically inert LiZn foil is much less and simple. The chemical degradation of the electrolyte on the Li foil would mainly generate inorganic species such as LiF and Li_2O and slight organic matter such as C-OR and COOR.

As for the study of the electrochemical degradation route, cyclic voltammetry (CV) was employed on the newly polished Li foil and LiZn foil ranging from 0 to 3 V for three cycles with a scanning rate of 0.1 mV s^{-1}. The cycled potential fluctuation of CV scanning is a simulation of that of the lithium plating/stripping process. For the polished Li foil, the formation of the SEI film is the coupling result of both the chemical and electrochemical degradation processes of the electrolyte (Figure 2c). In contrast, the LiZn foil acts as a chemically inert electrode to inquire into the pure electrochemical degradation of the electrolyte (Figure 2d). The electrochemical decomposition products of the Li foil and LiZn foil are almost the same, while the content of compositions is quite different. The C 1s spectra represent that the additional peak appears, which can be attributed to CO_3^{2-}(~291 eV) on the Li foil (Figure 2c);[34] meanwhile, the COOR and CO_3^{2-} are also generated on the LiZn foil (Figure 2d) after the electrochemical treatment. The remarkable augmentation of organic C-OR and COOR demonstrates that the organic matter mainly originates from the electrochemical degradation of the electrolyte. The occurrence of CO_3^{2-} can be ascribed to the electrochemical oxidation of C-OR and COOR species to Li_2CO_3. When the negative sweep of CV scanning is reversed, the C-OR and COOR could be partly oxidized and form Li_2CO_3.[38] In particular, the content of CO_3^{2-} on the Li foil is much higher than that on the LiZn foil, while the organic precursors C-OR and COOR are the dominant components on the LiZn foil after the electrochemical treatment. The further decomposition of C-OR and COOR to CO_3^{2-} can be obviously delayed by the LiZn alloy layer. F 1s spectra indicate that LiF is still the dominant component on the Li foil (Figure 2c) when the coupling chemical and electrochemical reactions occur together. However, when the chemical reaction is inhibited, the formation of LiF is obviously inhibited on the LiZn foil even after the electrochemical treatment (Figure 2d). The O 1s spectra also exhibit that when the chemical reaction is inhibited, further decomposition of the solvent is delayed, and the organic composition C-OR obviously increases on the LiZn foil.

Molecular dynamics (MD) simulation was used to represent the ion distribution near the LiZn interphase when different cathodic polarizations are applied on the electrode (Figure S2). When the electrode was maintained at the potential of zero charge (PZC), numerous PF_6^- ions were distributed in the Helmholtz layer (~5 Å), while the LiZn layer can prevent the decomposition. However, when cathodic polarization is applied, the PF_6^- is repelled out from the Helmholtz layer. When a polarization of −200 mV vs PZC is applied (Figure 2e), scarcely any PF_6^- is observed in the Helmholtz layer, implying that the reduction of PF_6^- and the relevant parasitic reaction are hard to occur. Hence, the solvent will be

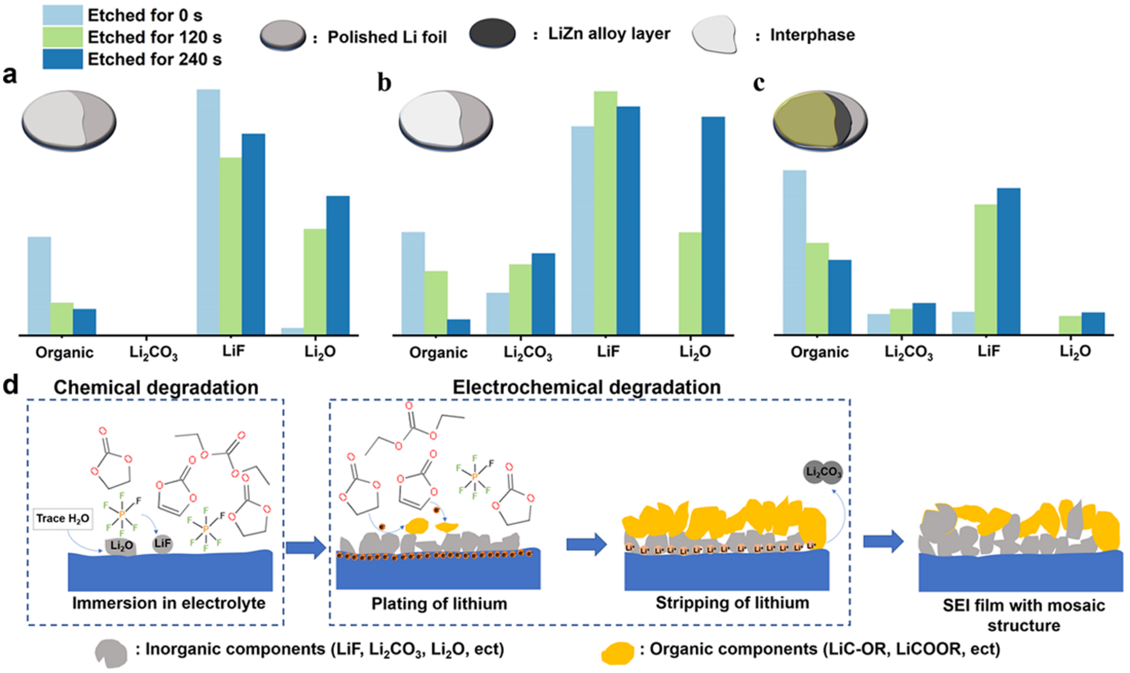

Figure 3. Depth profiles of the components on the surface of electrode. (a) Polished Li foil after exposing to the carbonate-based electrolyte for 72 h. (b) Polished Li foil after CV scanning for three cycles. (c) LiZn foil after CV scanning for three cycles. (d) Schematic of the formation mechanism of the common mosaic SEI film.

decomposed preferentially and formulate an organic layer during the electrochemical degradation.

In general, the chemical degradation of the electrolyte on the surface of lithium metal mainly would generate inorganic LiF and Li_2O and slight organic species. The uniform and dense LiZn alloy layer can significantly suppress the chemical degradation. With regard to electrochemical degradation, the solvent will mainly be decomposed into organic C-OR and COOR, which could be partly oxidized into Li_2CO_3. When the LiZn layer is introduced, the further decomposition of organic matters to Li_2CO_3 is also delayed. The preconstructed LiZn alloy layer can obviously inhibit the generation of inorganic species such as LiF, Li_2O, and Li_2CO_3 and increase the content of organic C-OR and COOR during the electrochemical treatment.

The different degradation routes of the electrolyte will also make distinct contribution to the structure of the SEI film. XPS analysis for different depths of the SEI film was applied to observe the constitution and structure of the SEI film after different treatments and explore the formation process of the SEI film, wherein some typical species are observed to speculate the degradation process of the electrolyte. Figure 3a−c represents the depth profile of typical organic matters (C-OR and COOR) and inorganic matters (Li_2CO_3, LiF, and Li_2O) on the surface of different electrodes, which is summarized by XPS spectra (Figure S3). Each electrode is etched using Ar for 0, 120, and 240 s. As for the LiZn foil after immersion, the XPS spectrum of the interphase after etching can be matched with the LiZn alloy (Figure S4), which represents that the generated film is too thin to be etched. For the Li foil after exposing to the electrolyte for 72 h (Figure 3a), the content of organic components such as C-OR and COOR gradually decreases, while the content of Li_2O obviously augments after etching. This manifests that the chemical degradation of the electrolyte will dramatically thicken the SEI film. The inhibition of chemical degradation by the LiZn layer can facilitate the lightness of the SEI film, relieving the interface impedance.

When CV scanning is employed on different electrodes, the constitution and structure of the interphase exhibit remarkable differences. After the electrochemical treatment, Figure 3b,c manifests that the content of Li_2CO_3 gradually increases after etching on both the Li foil and LiZn foil. During the electrochemical treatment, solvents are decomposed into organic C-OR and COOR during the preceding negative sweep. Subsequently, the organic matters can be oxidized into Li_2CO_3 when the polarization is switched to a positive sweep. This process is equivalent to the stripping of lithium in the wake of plating of lithium. The oxidation of organic matters will preferentially occur close to the electrode, leading to the higher content of Li_2CO_3 near the electrode. The O 1s spectrum of the surface of the LiZn foil after the electrochemical treatment (Figure 3d) exhibits that the generation of Li_2O remains minimal when chemical degradation is suppressed. However, when chemical degradation is not inhibited, the Li_2O species is equally extensive on the interphase of the Li foil, and the content of Li_2O obviously augments after etching. (Figure 3a,c). This manifests that the Li_2O mainly originates from the chemical degradation of the electrolyte, which highly relies on the active lithium. As for inorganic LiF, the distribution is irregular in the interphase of the Li foil after different treatments, while the generation of LiF on the LiZn foil is obviously inhibited. Cui and his collaborators[39] have observed the structure of the SEI film via cryo-STEM and found that LiF is absent within the compact SEI film. Instead, LiF particles (100−400 nm) precipitate across the electrode surface. This irregular distribution of LiF could be ascribed to the particles precipitated unevenly across the electrode surface. This process mainly roots in the chemical degradation of the electrolyte.

In summary, the formation of the SEI film can be described as the conjunct product of chemical and electrochemical

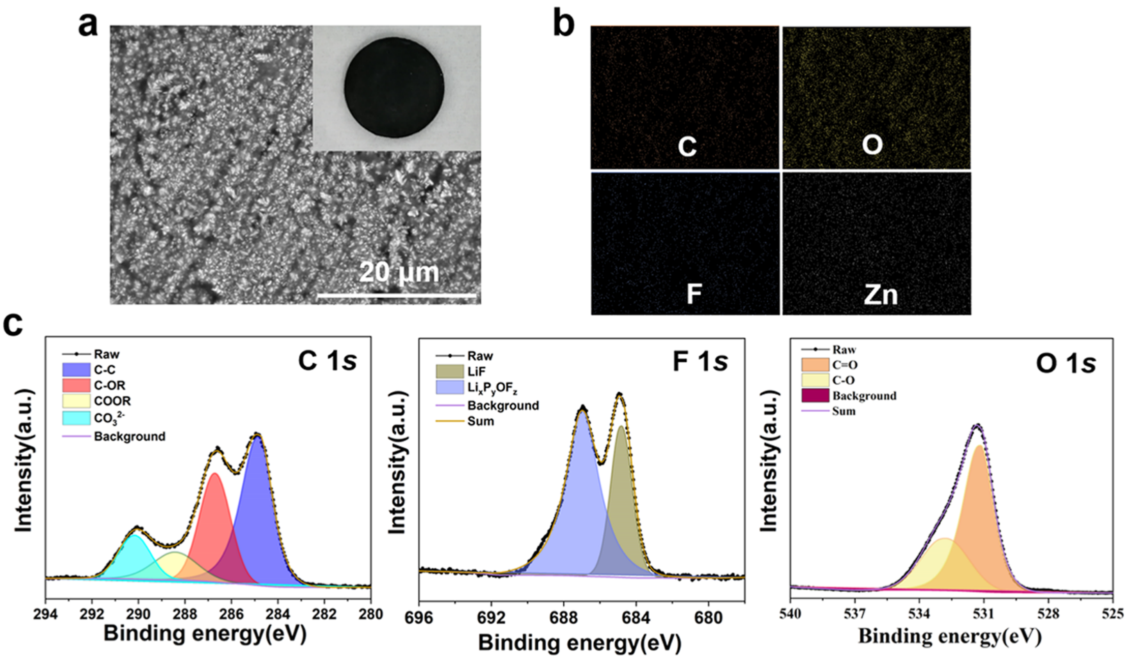

Figure 4. Optical and SEM image (a) and elemental mapping (b) of the DS-Li foil. (c) XPS spectrum of the surface of the DS-Li foil.

degradation of the electrolyte. The formation process of the SEI film is depicted in Figure 3d. When exposed to the electrolyte, the lithium metal could immediately react with the electrolyte to produce inorganic matters such as Li_2O and LiF, forming the inner layer. During the plating of lithium, the solvent will be decomposed to the outer organic layer containing C-OR and COOR. The organic matters could be partly oxidized to Li_2CO_3 during the following stripping of lithium. The further oxidization will preferentially occur close to the lithium and participate in the inner inorganic layer. It has to be pointed out that the chemical degradation will continuously occur along with the electrochemical degradation once a fresh lithium interface arises. Hence, the SEI film with a common mosaic model containing an inorganic inner layer and organic outer layer is obtained.

The distinction of chemical and electrochemical degradation provides an innovative perspective to explore the formation process of the SEI film, and the formation of the SEI film in carbonate electrolytes is illustrated. Although the idiographic degradation process is disparate in different electrolytes, the perspective of exploration can be extended to diverse electrolytes to dissect the formation process, which is vital to the regulation of the SEI film.

The electrochemical method is always considered as a commendable path to precisely regulate the SEI film, whereas the irrepressible chemical reaction hinders the regulation.[40,41] Based on this, the constitution and structure of the SEI film can be further regulated with a well-defined composition and structure by electrochemical modification.

Herein, the LiZn alloy layer which can induce the uniform deposition of lithium is constructed as a single-functional SEI film on the surface of the lithium foil (SS-Li foil). However, the LiZn layer as a single-functional SEI film is not desirable enough to facilitate the uniform plating/stripping of lithium after long cycling due to the poor electronic insulation and flexibility. Hence, a heterojunction-type SEI film with a dual-functional layer is further constructed by the electrochemical modification added to the SS-Li foil. Due to the inhibition of chemical degradation of the electrolyte by the LiZn layer, the outer layer could be lighter and consists of organic matters. As can be seen from the CV graph (Figure S5), the main reaction potential ranges from 1.1 to 1.6 V. In addition, little distinction of the CV graph is observed, indicating that the SS-Li foil exhibits similar potential variation to the Li foil. This manifests that the pretreated LiZn alloy layer does not alter the redox potential of the lithium anode, and it can still be applied in high-voltage batteries with high energy density. Herein, the outer layer is constructed by scanning CV from 1.1 to 1.6 V at a scanning rate of 0.5 mV s^{-1} for three cycles. Figure 4a,b represents that the surface of the LiZn layer is uniformly covered by a dark film, with C, O, and F species uniformly distributed, implying the successful formation of the outer organic layer. The XPS spectrum (Figure 4c) also represents that organic C-OR and COOR are the dominant compositions of the outer layer, and the content of the inorganic LiF and Li_2O is obviously suppressed in the outer layer. Overall, a highly organic outer layer was constructed on the surface of the LiZn layer. The outer layer constructed by electrochemical modification is similar to that of the native SEI film with great electronic insulation and good compatibility to the electrolyte. Additionally, the outer layer possesses a better elasticity modulus, which can accommodate the stress of volume change in the repeated lithium plating/striping process. Therefore, the Li foil with a dual-functional layer as a heterojunction-type SEI film (DS-Li foil) can not only induce the uniform deposition of lithium by the inner LiZn alloy layer but also suppress the continuous degradation of the electrolyte and accommodate the volume change during cycling by the outer organic layer. The synergistic effect of the heterojunction-type SEI film can facilitate the desirable cycle stability of the interphase. According to the Tafel curve (Figure S6), the exchange current density of the DS-Li foil (0.093 mA cm^{-2}) is slightly lower than that of the SS-Li foil (0.101 mA cm^{-2}). The constructed organic layer has a negligible effect on the ion transport kinetics of the interface, which will not hinder the fast ion transfer.

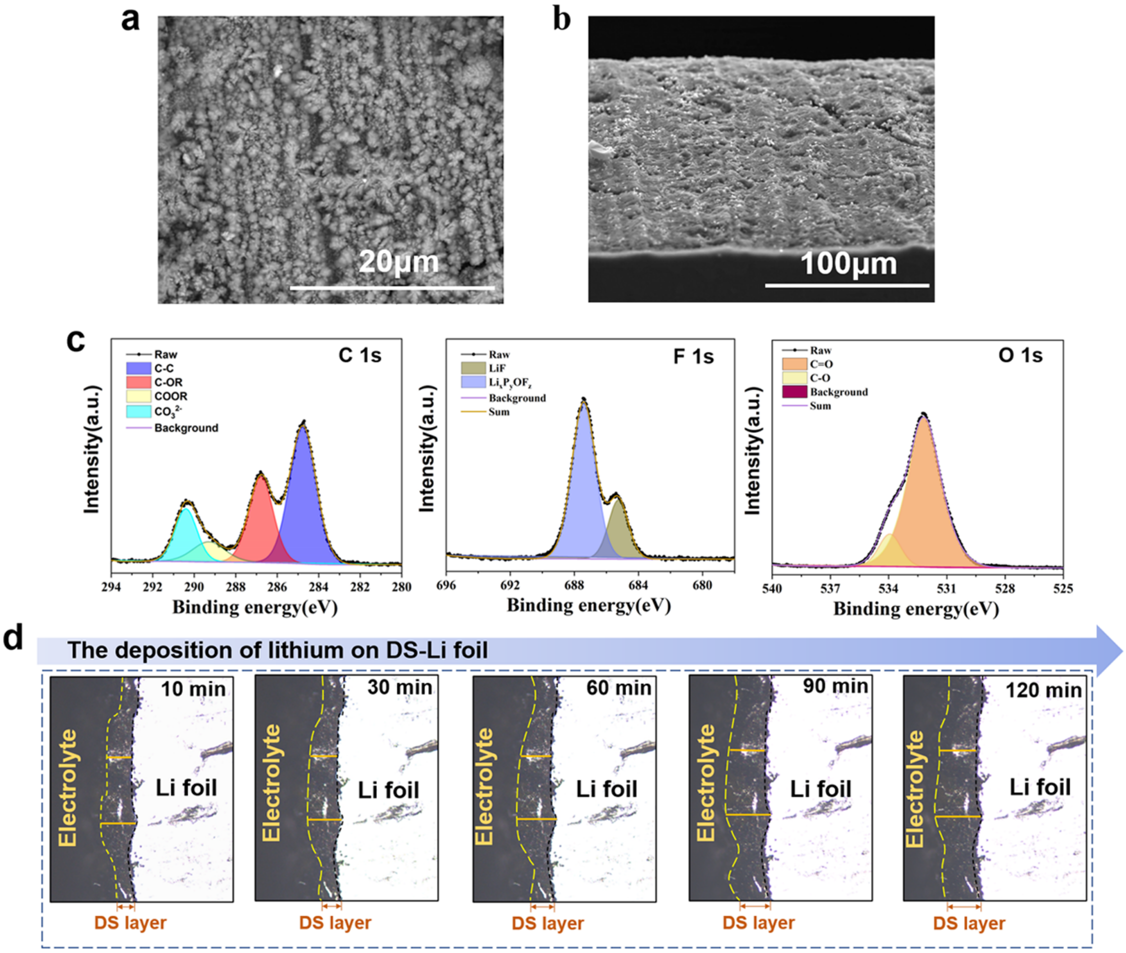

Figure 5. SEM images of the surface (a) and cross section (b) of DS-Li foil after plating with 2 mAh cm^{-2} lithium. (c) XPS spectrum of the DS-Li anode after plating with lithium of 2 mAh cm^{-2}. (d) In situ observation of the DS-Li foil when plating with lithium for different times at a current of 1 mAh cm^{-2}.

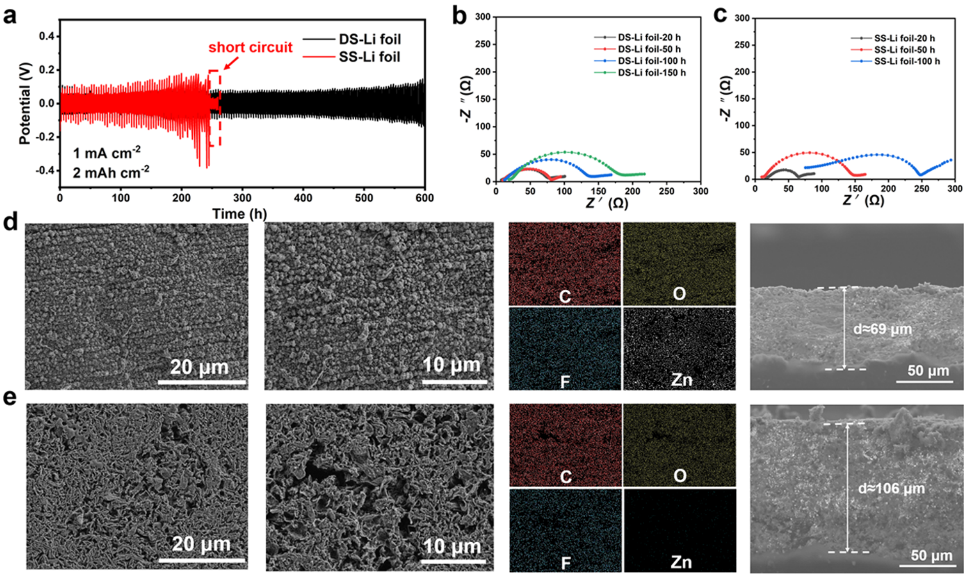

Figure 6. (a) Comparison of the cycling stability of the symmetric cells with the DS-Li electrode and SS-Li electrode at 1 mA cm^{-2} with a capacity of 2 mAh cm^{-2}. Nyquist plots of symmetric cells cycled for different times with the SS-Li electrode (b) and DS-Li electrode (c). The surface and cross-sectional morphology and the corresponding element mappings of the DS-Li electrode (d) and SS-Li electrode (e) after cycling for 100 h.

The stability of the interphase is vital for the utilization of the heterojunction-type SEI film. The plating/stripping of lithium should not destroy the preconstructed SEI film and form fresh lithium. To demonstrate the stability of the interphase, lithium was plated on the DS-Li foil at a current density of 1 mA cm^{-2} and a capacity of 2 mAh cm^{-2}. The surface morphology after deposition of lithium only exhibits little expansion compared to the surface of the DS-Li foil (Figure 5a), which indicates that the deposition of lithium will not form a fresh lithium interface and destroy the artificial SEI film. The cross profile (Figure 5b) also reveals that a fresh interface is not found after plating with 2 mAh cm^{-2} lithium. XPS analysis was also performed to confirm the stability of the interphase. Figure 5c displays the XPS spectrum of the modified anode after deposition of 2 mAh cm^{-2} lithium. The C 1s spectrum reveals that the C-OR and COOR still dominate after the deposition of lithium. As proved before, LiF will dominate in the SEI film of fresh lithium after the electrochemical treatment, whereas the F 1s spectrum demonstrates that the content of LiF remains slight, which also indicates that fresh lithium did not appear above the artificial SEI film. The O 1s spectrum also testifies the similar composition of the modified anode before and after the deposition of lithium. To further observe the deposition behavior of lithium, in situ observation was applied on the DS-Li foil when lithium was plated at a current density of 1 mA cm^{-2}. Figure 5d represents that the lithium layer gradually thickens without the generation of a fresh lithium layer, which attests that the artificial SEI film can maintain stability during the deposition of lithium. Thanks to the inner LiZn layer, which can induce the deposition of lithium through the interface, and the outer organic layer, which can inhibit the volume expansion, the preconstructed SEI film can maintain stability and play a role in facilitating the uniform plating/stripping of lithium during cycling. In contrast, mossy lithium is obtained on the surface of the SS-Li foil after deposition of 2 mAh cm^{-2} lithium (Figure S7a), and a mass of LiF is observed on the surface (Figure S7b), manifesting the generation of fresh lithium. In addition, the in situ observation of the SS-Li foil represents that the deposited lithium will result in rapid and uncontrolled volume expansion without the synergistic effect of the outer organic layer.

To verify whether the heterojunction-type SEI film can promote the uniform plating/stripping of lithium, the DS-Li foil and SS-Li foil were assembled into symmetric cells using a carbonate electrolyte. The polarization voltage plots are shown in Figure 6. Figure 6a represents that the cell with the DS-Li electrode can be stably cycled for over 600 h with a low hysteresis voltage (~80 mV) at a current density of 1 mA cm^{-2} and a capacity of 2 mAh cm^{-2}. The uncontrollable thickening of the SEI film could deteriorate ion transfer kinetics and induce the heterogeneous growth of lithium. This finally results in the generation of lithium dendrites until they pierce the separator, resulting in a short circuit. In contrast, the hysteresis voltage of the DS-Li electrode can stabilize at a low value during repeated plating/stripping of lithium. The plating/stripping test of different currents and capacities was also conducted (Figure S8). The DS-Li electrode also exhibited better cycling performance. The heterojunction-type SEI film with dual-functional layers can not only induce the uniform deposition of lithium by the inner LiZn layer but also stabilize the interphase through the inhibition of electrochemical degradation of the electrolyte and volume change. The EIS test was also employed to reveal the interface characteristics of different anodes. The Nyquist plots (Figure 6b,c) with one semicircle can be interpreted using series-wound equivalent analogues of retractor−capacitor (RC) circuits, while the semicircle diameter is proportional to the interface impedance of the SEI film. In the beginning, the interface impedance of the DS-Li electrode is slightly greater than that of the SS-Li electrode, which could be ascribed to the preconstructed organic layer. However, after cycling for 50 and 100 h, the interface impedance of the SS-Li electrode violently increases, while the interface impedance of the DS-Li electrode can hold steady even after 150 h.

The morphology of the SS-Li electrode and DS-Li electrode after cycling for 100 h was observed. Figure 6e reveals that the LiZn layer has been smashed and the "dead" lithium whiskers remain at the surface of the electrode. The whisker-shaped "dead" lithium cannot be utilized again, which will deteriorate the cycling performance of the electrode and result in the evolution of dendrites. The corresponding elemental mapping reveals that the Zn element is rare at the surface, indicating that the LiZn layer has been completely destroyed. In contrast, the morphology of the DS-Li electrode can remain intact even after cycling for 100 h (Figure 6d). The corresponding elemental mapping also manifests that the heterojunction-type SEI film can remain undestroyed after cycling for 100 h. The cross profiles reveal that a foamy "dead lithium" layer with a thickness of 106 μm was observed in the SS-Li electrode after cycling for 100 h (Figure 6e). The foamy lithium is too loose to be stripped again, which can result in the loss of capacity. However, the cross profile of the DS-Li electrode can remain compact with a thickness of only 69 μm (Figure 6d). The heterojunction-type SEI film can make up the weakness of the single LiZn layer, inhibiting the uncontrollable thickening of the SEI film. In addition, the outer organic layer is flexible enough to accommodate the volume change during cycling and suppress the generation of "dead lithium" and dendrites. Hence, the heterojunction-type SEI film can facilitate the excellent long cycling performance of the lithium anode in a carbonate electrolyte.

The DS-Li foil was also assembled as a full cell with $LiNi_{0.5}Co_{0.2}Mn_{0.3}O_2$ to study the compatibility of the modified anode and high-voltage cathode. Figure S9a reveals that the full cell with the DS-Li anode can maintain a discharge capacity of 85.6% with a reversible discharge capacity of 138 mAh g^{-1} after 400 cycles at 1C, with a cutoff voltage ranging from 2.75 to 4.3 V. The capacity−voltage curve (Figure S9b) also manifests that the full cell with the DS-Li foil as an anode has excellent reversibility. The artificial heterojunction-type SEI film demonstrates great compatibility with high-voltage cathodes, which is crucial to exert the high capacity of the lithium metal anode.

The improved performance of the DS-Li foil manifests that it is feasible to accurately regulate the components and structure of the SEI film based on the distinction of chemical and electrochemical degradation of the electrolyte. This provides us an innovative perspective to cognize and regulate the SEI film.

CONCLUSIONS

In general, a uniform and dense LiZn layer is constructed on the Li foil by a simple chemical method, which acts as a chemically inert but electrochemically active interphase. Based on this, the chemical and electrochemical degradation in a carbonate electrolyte was distinguished and explored separately. The distinction of chemical and electrochemical degradation of the electrolyte facilitates the precise regulation of the SEI film via electrochemical modification. Herein, a heterojunction-type SEI film is further constructed by electrochemical modification when inorganic matters (LiF, Li_2O, and Li_2CO_3) are tellingly suppressed. Therefore, the modified anode exhibits excellent cycle stability—over 600h with a low hysteresis voltage (~80 mV) at a current density of 1 mA cm^{-2} and a capacity of 2 mAh cm^{-2}—in carbonate-based electrolytes. The improved performance of the DS-Li foil manifests that the components and structure of the SEI film can be further regulated based on the distinction of chemical and electrochemical degradation of the electrolyte to promote the performance of the Li anode. This work provides an innovate perspective to explore the formation of the SEI film via the distinction of the chemical and electrochemical degradation of the electrolyte. This contributes to the further understanding of the SEI film and accurate regulation of the artificial SEI film to promote the application of lithium metal batteries.

■ ASSOCIATED CONTENT

Supporting Information

The Supporting Information is available free of charge at https://pubs.acs.org/doi/10.1021/acssuschemeng.2c02668.

Nyquist plots, ion distribution, XPS spectra, CV curves, Tafel curves, SEM images, in situ observation, cycling performance of the symmetric cells, Coulomb efficiency, and capacity curve of the full cell (PDF)

■ AUTHOR INFORMATION

Corresponding Authors

Peng Zhang − *College of Energy, Xiamen University, Xiamen 361102, P. R. China*; Email: pengzhang@xmu.edu.cn

Jinbao Zhao − *College of Energy, Xiamen University, Xiamen 361102, P. R. China; State-Province Joint Engineering Laboratory of Power Source Technology for New Energy Vehicle Engineering Research Center of Electrochemical Technology Ministry of Education College of Chemistry and Chemical Engineering, Xiamen University, Xiamen 361005, P. R. China*; orcid.org/0000-0002-2753-7508; Email: jbzhao@xmu.edu.cn

Authors

Jiaxiang Liu − *College of Energy, Xiamen University, Xiamen 361102, P. R. China*

Nanbiao Pei − *College of Energy, Xiamen University, Xiamen 361102, P. R. China*

Haiming Hua − *College of Chemistry and Chemical Engineering, Xiamen University, Xiamen 361005, P. R. China*

Yi Deng − *College of Energy, Xiamen University, Xiamen 361102, P. R. China*

Haoshen Ma − *College of Energy, Xiamen University, Xiamen 361102, P. R. China*

Complete contact information is available at: https://pubs.acs.org/10.1021/acssuschemeng.2c02668

Notes

The authors declare no competing financial interest.

■ ACKNOWLEDGMENTS

The authors gratefully acknowledge financial support from the National Natural Science Foundation of China (Grant Nos. 21875195, 21875198, and 22005257) and the Fundamental Research Funds for the Central Universities (20720190040). The authors also would like to express gratitude to the support of Tan Kah Kee Innovation Laboratory. The authors appreciate the positive discussion and advices from Prof. Zhou Yao from Xiamen University and Prof. Fu Lijun from Nanjing Tech University.

■ REFERENCES

(1) Cheng, X.-B.; Zhang, R.; Zhao, C.-Z.; Zhang, Q. Toward Safe Lithium Metal Anode in Rechargeable Batteries: A Review. *Chem. Rev.* **2017**, *117*, 10403−10473.

(2) Chai, Y.; Zheng, S.; Zhao, W.; Fan, J.; Shi, P.; Xu, Q.; Min, Y. Regulating the Interfacial Electric Field for a Stable Lithium Metal Anode. *ACS Sustainable Chem. Eng.* **2022**, *10*, 956−966.

(3) Bi, Z.; Guo, X. Solidification for solid-state lithium batteries with high energy density and long cycle life. *Energy Mater.* **2022**, *2*, No. 200011.

(4) Mao, H.; Yu, W.; Cai, Z.; Liu, G.; Liu, L.; Wen, R.; Su, Y.; Kou, H.; Xi, K.; Li, B.; Zhao, H.; Da, X.; Wu, H.; Yan, W.; Ding, S. Current-Density Regulating Lithium Metal Directional Deposition for Long Cycle-Life Li Metal Batteries. *Angew. Chem., Int. Ed.* **2021**, *60*, 19306−19313.

(5) Zhao, C.-Z.; Duan, H.; Huang, J.-Q.; Zhang, J.; Zhang, Q.; Guo, Y.-G.; Wan, L.-J. Designing solid-state interfaces on lithium-metal anodes: a review. *Sci. China Chem.* **2019**, *62*, 1286−1299.

(6) Xiong, X.; Yan, W.; Zhu, Y.; Liu, L.; Fu, L.; Chen, Y.; Yu, N.; Wu, Y.; Wang, B.; Xiao, R. Li4Ti5O12 Coating on Copper Foil as Ion Redistributor Layer for Stable Lithium Metal Anode. *Adv. Energy Mater.* **2022**, *12*, No. 2103112.

(7) Li, S.; Luo, Z.; Li, L.; Hu, J.; Zou, G.; Hou, H.; Ji, X. Recent progress on electrolyte additives for stable lithium metal anode. *Energy Storage Mater.* **2020**, *32*, 306−319.

(8) Zhai, P.; Wang, T.; Jiang, H.; Wan, J.; Wei, Y.; Wang, L.; Liu, W.; Chen, Q.; Yang, W.; Cui, Y.; Gong, Y. 3D Artificial Solid-Electrolyte Interphase for Lithium Metal Anodes Enabled by Insulator−Metal−Insulator Layered Heterostructures. *Adv. Mater.* **2021**, *33*, No. 2006247.

(9) Peng, X.; Wang, C.; Liu, Y.; Fang, W.; Zhu, Y.; Fu, L.; Ye, J.; Liu, L.; Wu, Y. Critical advances in re-engineering the cathode-electrolyte interface in alkali metal-oxygen batteries. *Energy Mater.* **2021**, *1*, No. 100011.

(10) Sacci, R. L.; Dudney, N. J.; More, K. L.; Parent, L. R.; Arslan, I.; Browning, N. D.; Unocic, R. R. Direct visualization of initial SEI morphology and growth kinetics during lithium deposition by in situ electrochemical transmission electron microscopy. *Chem. Commun.* **2014**, *50*, 2104−2107.

(11) Zeng, Z.; Liang, W.-I.; Liao, H.-G.; Xin, H. L.; Chu, Y.-H.; Zheng, H. Visualization of electrode−electrolyte interfaces in LiPF6/EC/DEC electrolyte for lithium ion batteries via in situ TEM. *Nano Lett.* **2014**, *14*, 1745−1750.

(12) Lin, S.; Hua, H.; Lai, P.; Zhao, J. A Multifunctional Dual-Salt Localized High-Concentration Electrolyte for Fast Dynamic High-Voltage Lithium Battery in Wide Temperature Range. *Adv. Energy Mater.* **2021**, *11*, No. 2101775.

(13) Tan, S. J.; Wang, W. P.; Tian, Y. F.; Xin, S.; Guo, Y. G. Advanced Electrolytes Enabling Safe and Stable Rechargeable Li-Metal Batteries: Progress and Prospects. *Adv. Funct. Mater.* **2021**, *31*, No. 2105253.

(14) Cui, X.; Chu, Y.; Qin, L.; Pan, Q. Stabilizing Li Metal Anodes through a Novel Self-Healing Strategy. *ACS Sustainable Chem. Eng.* **2018**, *6*, 11097−11104.

(15) Peled, E.; Golodnitsky, D.; Ardel, G. Advanced model for solid electrolyte interphase electrodes in liquid and polymer electrolytes. *J. Electrochem. Soc.* **1997**, *144*, L208.

(16) Kanamura, K.; Tamura, H.; Shiraishi, S.; Takehara, Z.-i. XPS analysis of lithium surfaces following immersion in various solvents containing LiBF4. *J. Electrochem. Soc.* **1995**, *142*, 340.

(17) Chen, J.; Li, Q.; Pollard, T. P.; Fan, X.; Borodin, O.; Wang, C. Electrolyte design for Li metal-free Li batteries. *Mater. Today* **2020**, *39*, 118−126.

(18) Cheng, X. B.; Zhang, R.; Zhao, C. Z.; Wei, F.; Zhang, J. G.; Zhang, Q. A review of solid electrolyte interphases on lithium metal anode. *Adv. Sci.* **2016**, *3*, No. 1500213.

(19) Boyle, D. T.; Huang, W.; Wang, H.; Li, Y.; Chen, H.; Yu, Z.; Zhang, W.; Bao, Z.; Cui, Y. Corrosion of lithium metal anodes during calendar ageing and its microscopic origins. *Nat. Energy* **2021**, *6*, 487−494.

(20) Lin, D.; Liu, Y.; Li, Y.; Li, Y.; Pei, A.; Xie, J.; Huang, W.; Cui, Y. Fast galvanic lithium corrosion involving a Kirkendall-type mechanism. *Nat. Chem.* **2019**, *11*, 382−389.

(21) Kolesnikov, A.; Kolek, M.; Dohmann, J. F.; Horsthemke, F.; Börner, M.; Bieker, P.; Winter, M.; Stan, M. C. Lithium Metal Batteries: Galvanic Corrosion of Lithium-Powder-Based Electrodes (Adv. Energy Mater. 15/2020). *Adv. Energy Mater.* **2020**, *10*, No. 2070065.

(22) Bayly, C. I.; Cieplak, P.; Cornell, W.; Kollman, P. A. A Well-Behaved Electrostatic Potential Based Method Using Charge Restraints for Deriving Atomic Charges: The RESP Model. *J. Phys. Chem. A* **1993**, *97*, 10269.

(23) Grimme, S.; Antony, J.; Ehrlich, S.; Krieg, H. A consistent and accurate ab initio parametrization of density functional dispersion correction (DFT-D) for the 94 elements H-Pu. *J. Chem. Phys.* **2010**, *132*, No. 154104.

(24) Stephens, P. J.; Devlin, F. J.; Chabalowski, C. F.; Frisch, M. J. Ab Initio Calculation of Vibrational Absorption and Circular Dichroism Spectra Using Density Functional Force Fields. *J. Phys. Chem. B* **1994**, *98*, 11623.

(25) Weigend, F.; Ahlrichs, R. Balanced basis sets of split valence, triple zeta valence and quadruple zeta valence quality for H to Rn: Design and assessment of accuracy. *Phys. Chem. Chem. Phys.* **2005**, *7*, 3297−3305.

(26) Frisch, M. J.; Trucks, G. W.; Schlegel, H. B.; Scuseria, G. E.; Robb, M. A.; Cheeseman, J. R.; Scalmani, G.; Barone, V.; Mennucci, B.; Petersson, G. A.. *Gaussian 09*, Revision E.01; Gaussian, Inc.: Wallingford CT, 2013.

(27) Lu, T.; Chen, F. Multiwfn: a multifunctional wavefunction analyzer. *J. Comput. Chem.* **2012**, *33*, 580−592.

(28) Zhang, J.; Lu, T. Efficient evaluation of electrostatic potential with computerized optimized code. *Phys. Chem. Chem. Phys.* **2021**, *23*, 20323−20328.

(29) Abraham, M. J.; Murtola, T.; Schulz, R.; Páll, S.; Smith, J. C.; Hess, B.; Lindahl, E. GROMACS: High performance molecular simulations through multi-level parallelism from laptops to supercomputers. *SoftwareX* **2015**, *1−2*, 19−25.

(30) Sousa da Silva, A. W.; Vranken, W. F. ACPYPE - AnteChamber PYthon Parser interfacE. *BMC Res. Notes* **2012**, *5*, 367.

(31) Humphrey, W.; Dalke, A.; Schulten, K. VMD: visual molecular dynamics. *J. Mol. Graphics* **1996**, *14*, 33−38.

(32) Lin, Y.; Wen, Z.; Yang, C.; Zhang, P.; Zhao, J. Strengthening dendrite suppression in lithium metal anode by in-situ construction of Li−Zn alloy layer. *Electrochem. Commun.* **2019**, *108*, No. 106565.

(33) Le, Y.; Zhong, H.; Yang, Y.; He, R.; Yao, G.; Jin, F. Mechanism study of reduction of CO2 into formic acid by in-situ hydrogen produced from water splitting with Zn: Zn/ZnO interface autocatalytic role. *J. Energy Chem.* **2017**, *26*, 936−941.

(34) Li, N. W.; Shi, Y.; Yin, Y. X.; Zeng, X. X.; Li, J. Y.; Li, C. J.; Wan, L. J.; Wen, R.; Guo, Y. G. A flexible solid electrolyte interphase layer for long-life lithium metal anodes. *Angew. Chem., Int. Ed.* **2018**, *57*, 1505−1509.

(35) Qian, J.; Xu, W.; Bhattacharya, P.; Engelhard, M.; Henderson, W. A.; Zhang, Y.; Zhang, J.-G. Dendrite-free Li deposition using trace-amounts of water as an electrolyte additive. *Nano Energy* **2015**, *15*, 135−144.

(36) Jiao, S.; Zheng, J.; Li, Q.; Li, X.; Engelhard, M. H.; Cao, R.; Zhang, J.-G.; Xu, W. Behavior of lithium metal anodes under various capacity utilization and high current density in lithium metal batteries. *Joule* **2018**, *2*, 110−124.

(37) Liu, T.; Lin, L.; Bi, X.; Tian, L.; Yang, K.; Liu, J.; Li, M.; Chen, Z.; Lu, J.; Amine, K.; et al. In situ quantification of interphasial chemistry in Li-ion battery. *Nat. Nanotechnol.* **2019**, *14*, 50−56.

(38) Liu, T.; Lin, L.; Bi, X.; Tian, L.; Yang, K.; Liu, J.; Li, M.; Chen, Z.; Lu, J.; Amine, K.; Xu, K.; Pan, F. In situ quantification of interphasial chemistry in Li-ion battery. *Nat. Nanotechnol.* **2019**, *14*, 50−56.

(39) Huang, W.; Wang, H.; Boyle, D. T.; Li, Y.; Cui, Y. Resolving Nanoscopic and Mesoscopic Heterogeneity of Fluorinated Species in Battery Solid-Electrolyte Interphases by Cryogenic Electron Microscopy. *ACS Energy Lett.* **2020**, *5*, 1128−1135.

(40) Liu, Q. C.; Xu, J. J.; Yuan, S.; Chang, Z. W.; Xu, D.; Yin, Y. B.; Li, L.; Zhong, H. X.; Jiang, Y. S.; Yan, J. M.; Zhang, X. B. Artificial protection film on lithium metal anode toward long-cycle-life lithium−oxygen batteries. *Adv. Mater.* **2015**, *27*, 5241−5247.

(41) Ma, L.; Kim, M. S.; Archer, L. A. Stable artificial solid electrolyte interphases for lithium batteries. *Chem. Mater.* **2017**, *29*, 4181−4189.

https://doi.org/10.1021/acssuschemeng.2c02668